Collisional flavor swap with neutrino self-interactions

Chinami Kato[*]

Faculty of Science and Technology, Tokyo University of Science,
2641 Yamazaki, Noda-shi, Chiba 278-8510, Japan

Hiroki Nagakura

National Astronomical Observatory of Japan, 2-21-1 Osawa, Mitaka, Tokyo 181-8588, Japan

Lucas Johns

Departments of Astronomy and Physics, University of California, Berkeley, California 94720, USA

Neutrinos play pivotal roles in determining fluid dynamics, nucleosynthesis, and their observables in core-collapse supernova (CCSN) and binary neutron star merger (BNSM). In this paper, we present a novel phenomenon, collisional flavor swap, in which neutrino-matter interactions trigger the complete interchange of neutrino spectra between two different flavors, aided by neutrino self-interactions. We find that a necessary condition to trigger the collisional swap is occurrences of resonancelike collisional flavor instability. In cases where neutrino self-interactions substantially dominate over the collision rate, the collisional swap occurs in the entire neutrino energy spectrum, while intriguing energy-dependent features can emerge after the completion of flavor swap. Since flavor swaps correspond to the most extreme case in flavor conversions, they have a great potential to affect CCSN and BNSM phenomena.

I. INTRODUCTION

Exploring neutrino-flavor conversions driven by neutrino self-interactions (collective neutrino oscillations) [1–4] is a key frontier in the study of core-collapse supernovae (CCSNe) and binary neutron star mergers (BNSMs). The detailed investigation has been motivated by theoretical indications that flavor conversions ubiquitously occur in CCSN [5–18] and BNSM [19–25] environments. Their physical properties, however, remain shrouded in a mystery, despite their growing attention.

Some recent studies have also suggested that collisional flavor instability (CFI), a new type of collective neutrino oscillations, can occur in optically thick regions of CCSNe [17,26] and BNSMs [27]. Our understanding of CFI has been matured rapidly based on linear stability analysis (see, e.g., [27,28]), but much less work has been done on their nonlinear properties. We also note that the previous studies have ignored diagonal components of collision terms [29–31], which potentially discards some important characteristics of CFI. In fact, we shall show that the diagonal components play a pivotal role in characterizing nonlinear dynamics of CFI.

In this paper, we present a novel phenomenon in nonlinear phases of neutrino-flavor conversions, named as collisional flavor swap (or collisional swap). Here we use "swap" to refer to the simultaneous interchange of different flavors, i.e., more extreme than the flavor equipartition. There are two noticeable properties in collisional swap: (1) the timescale is much faster than neutrino-matter interactions, since the growth of flavor conversions in the early phase is associated with the resonancelike CFI [27,28]; (2) the collisional swap can occur in isotropic neutrino distributions in momentum space, indicating that the interplay with fast neutrino-flavor conversion is not necessary [30].

We stress that the collisional swap is distinct from other swap phenomena in the literature such as spectral swap [32,33] and Mikheyev–Smirnov-Wolfenstein effects. Occurrences of rapid and vigorous flavor conversions by CFI in regions where neutrinos and matter are strongly coupled can affect all relevant physics in these phenomena, including fluid dynamics, nucleosynthesis, and observable signals such as gravitational waves and neutrinos [34–39]. This exhibits the possibility of a large impact of collisional swap on both theories and observations for CCSNe and BNSMs.

II. DYNAMICAL SIMULATIONS

We start with presenting results of dynamical simulations for collisional swap by solving quantum kinetic equations (QKEs) of neutrinos. We solve the energy-dependent

*[*]ckato@rs.tus.ac.jp

TABLE I.   Setups in our model.

Density	Temperature	Electron fraction	Chemical potential
10^{12} g/cm^{-3}	6.4 MeV	0.1	0 MeV (ν_e, $\bar{\nu}_e$), -2 MeV (ν_x, $\bar{\nu}_x$)

QKEs under isotropic and spatial homogeneous neutrino background,

$$i\frac{\partial}{\partial t}\rho(t, E_\nu) = [H_{\nu\nu}, \rho(t, E_\nu)] + iC, \qquad (1)$$

with the density matrix ρ, neutrino energy E_ν, collision term C, and Hamiltonian potential,

$$H_{\nu\nu} = \sqrt{2}G_F \int dV_q[\rho(t, E_\nu) - \bar{\rho}^*(t, E_\nu)]. \qquad (2)$$

G_F and V_q are the Fermi constant and the volume element in momentum space, respectively. In this study, we neglect vacuum and matter potentials just for simplicity. We also assume the two-flavor system consisting of electron neutrinos (ν_e) and heavy-leptonic neutrinos (ν_x), in which case ρ is a 2×2 matrix, i.e.,

$$\rho = \begin{pmatrix} \rho_{ee} & \rho_{ex} \\ \rho_{xe} & \rho_{xx} \end{pmatrix}. \qquad (3)$$

For antineutrinos, we use "-" expression and replace $\rho \rightarrow \bar{\rho}$, $C \rightarrow \bar{C}$, and $H_{\nu\nu} \rightarrow \bar{H}_{\nu\nu} = -H^*_{\nu\nu}$ in Eqs. (1) and (2).

In the collision term, the electron and positron captures by free protons and neutrons, respectively, are included as emission processes, while absorption processes are also taken into account by their inverse reactions. ν_x reactions are not included in this study. Reaction rates of these processes are computed by following [40] under given a fluid distribution. Baryon mass density, temperature, and electron fraction are set as 10^{12} g/cm^3, 6.4 MeV, and 0.1, respectively (see Table I), while the similar matter state has been observed in recent CCSN models [41]. We also note that these parameters are chosen so that the ν_e chemical potential becomes zero, which corresponds to a necessary condition for occurrences of a resonancelike evolution in CFI [unless number densities of ν_x and their antipartner ($\bar{\nu}_x$) are largely different from each other, although these cases are not considered in this paper]. We employ a nuclear equation of state [42] to obtain all necessary thermodynamical quantities for computing weak reaction rates.

As an initial condition, we assume that ν_e and $\bar{\nu}_e$ are in thermal and chemical equilibrium with matter, whereas ν_x and $\bar{\nu}_x$ are assumed to be Fermi-Dirac distributions with the chemical potential of -2 MeV. The choice of the chemical potential of ν_x is based on our CCSN model [43]. We consider the region outside the energy sphere, at which neutrino emission and absorption are balanced with

each other.[1] In this region, ν_x and $\bar{\nu}_x$ undergo large numbers of scatterings mainly by nucleons, which leads to the negative chemical potential [45]. It should be noted, however, that the ν_x radiation field is sensitive to neutrino-matter interactions and multidimensional effects such as proto-neutron star convection [46], which would affect occurrences of CFI [26,47]. It is, hence, necessary to inspect ν_x when we assess occurrences of collisional swap in CCSN models. We add very small perturbations in off-diagonal components of density matrix (10^{-6} compared to electron-type neutrinos) to trigger flavor conversions.

We assess the stability of neutrino distributions by following the prescription in [28] and confirm that CFI occurs with the growth rate of 5×10^{-3} cm^{-1}. The associated timescale of CFI (t_{CFI}) is $\sim 10^{-5}$ shorter than the timescale of neutrino-matter interaction (t_{col}). This exhibits that the flavor instability corresponds to a resonancelike CFI, whose timescale can be roughly estimated as $t_{CFI} \sim \sqrt{G_F n_\nu \gamma}$, where n_ν and γ denote the number density of neutrinos and energy-averaged reaction rates of neutrino-matter interactions, respectively. We solve the QKEs by using the Monte Carlo code [48], in which we employ a uniform energy grid from 0 to 100 MeV with 100 grid points. We also carry out the same simulation but with twice the energy resolution (200 grids). We find that the result is almost identical to that with our standard resolution (the error of neutrino number density is less than 0.1%). Hence, we hereafter discuss the collisional swap based on the model with the standard resolution.

Solid lines in Fig. 1 draw the dynamics of collisional swap, while we omit to show those in antineutrinos, since their evolution is almost identical to neutrinos. ν_e and ν_x substantially shuffle at $t \sim 2 \times 10^{-8}$ s, and then the flavor swap almost completes by $t \sim 1 \times 10^{-7}$ s.

Before discussing the physical process of collisional swap in detail, we make an interesting comparison to the case with no collision term in diagonal elements; the results are shown as dotted lines in Fig. 1. In the early phase, the time evolution of flavor conversions is almost identical to the case with diagonal collision terms, which is consistent with linear analysis. However, they deviate from each other

---

[1]We follow the convection in [44], which distinguishes energy and transport spheres for ν_x (and $\bar{\nu}_x$). Unlike ν_e and $\bar{\nu}_e$, there is a scattering dominant region. In such a region, they are not in thermal and chemical equilibrium with matter, but their angular distributions are nearly isotropic due to scatterings with nucleons. The transport (or scattering) sphere is located outside the energy one, and it is defined as the sphere where ν_x transits to free streaming.
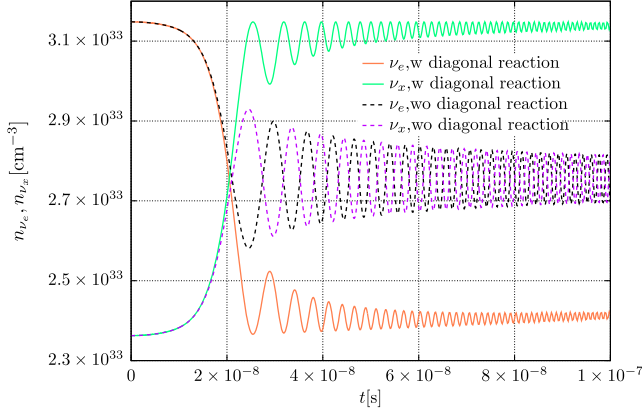
FIG. 1. Time evolution of number densities of neutrinos. Red and green solid lines denote ν_e and ν_x (n_{ν_e} and n_{ν_x}), respectively. Solid and dotted lines denote cases with (w) and without (wo) diagonal components of collision terms, respectively; see text for more details.

from $t \sim 2 \times 10^{-8}$ s, corresponding to the time when the number of neutrinos of two flavors become nearly equal. In the case without diagonal collision terms, the system converges to a flavor equipartition with oscillations. This exhibits that the diagonal elements in collision terms are key elements to understand collisional swap, which can also be shown analytically (see below).

III. ANALYTIC ARGUMENTS

We discuss the collisional swap in terms of polarization vectors in flavor spaces, which are defined by $\rho \equiv P_0 I/2 + \boldsymbol{P} \cdot \boldsymbol{\sigma}/2$ with

$$\boldsymbol{P} = (2\mathrm{Re}\rho_{ex}, -2\mathrm{Im}\rho_{ex}, \rho_{ee} - \rho_{xx}), \quad (4)$$

$$\bar{\boldsymbol{P}} = (2\mathrm{Re}\bar{\rho}_{ex}, 2\mathrm{Im}\bar{\rho}_{ex}, \bar{\rho}_{ee} - \bar{\rho}_{xx}), \quad (5)$$

$P_0 = \rho_{ee} + \rho_{xx}$, the unit matrix I, and the Pauli matrix vector $\boldsymbol{\sigma}$. It should be mentioned that $\boldsymbol{P}$ and $\bar{\boldsymbol{P}}$ depend on neutrino energy. In this expression, the QKEs are

$$\frac{\partial}{\partial t}\boldsymbol{P} = \boldsymbol{H}_{\nu\nu} \times \boldsymbol{P} + \Gamma(\boldsymbol{P}_{\mathrm{eq}} - \boldsymbol{P}) + \Gamma(P_{0,\mathrm{eq}} - P_0)\boldsymbol{z}, \quad (6)$$

$$\frac{\partial}{\partial t}\bar{\boldsymbol{P}} = \boldsymbol{H}_{\nu\nu} \times \bar{\boldsymbol{P}} + \bar{\Gamma}(\bar{\boldsymbol{P}}_{\mathrm{eq}} - \bar{\boldsymbol{P}}) + \bar{\Gamma}(\bar{P}_{0,\mathrm{eq}} - \bar{P}_0)\boldsymbol{z}, \quad (7)$$

with $\Gamma = \Gamma_e/2$ and $\bar{\Gamma} = \bar{\Gamma}_e/2$; Γ_e ($\bar{\Gamma}_e$) denotes the reaction rate for ν_e (electron antineutrinos $\bar{\nu}_e$), while we consider the situation with $\Gamma > \bar{\Gamma}$ due to neutron rich environment; $\boldsymbol{z}$ is the unit vector of the z axis in flavor space; the index "eq" indicates the quantities in the thermal equilibrium. The Hamiltonian vector is

$$\boldsymbol{H}_{\nu\nu} = \mu \int dV_q(\boldsymbol{P} - \bar{\boldsymbol{P}}), \quad (8)$$

with $\mu = \sqrt{2}G_F$.

To capture the essential features of collisional swap, we consider an energy-integrated form of the QKE, while the detailed discussion about energy dependence is deferred to Sec. IV. The QKEs can be approximated as

$$\frac{\partial}{\partial t}\boldsymbol{P}_{\mathrm{int}} \sim -\mu\bar{\boldsymbol{P}}_{\mathrm{int}} \times \boldsymbol{P}_{\mathrm{int}} + \Gamma_{\mathrm{ave}}(\boldsymbol{P}_{\mathrm{int,eq}} - \boldsymbol{P}_{\mathrm{int}})$$
$$+ \Gamma_{\mathrm{ave}}(P_{0\mathrm{int,eq}} - P_{0\mathrm{int}})\boldsymbol{z}, \quad (9)$$

$$\frac{\partial}{\partial t}\bar{\boldsymbol{P}}_{\mathrm{int}} \sim -\mu\bar{\boldsymbol{P}}_{\mathrm{int}} \times \boldsymbol{P}_{\mathrm{int}} + \bar{\Gamma}_{\mathrm{ave}}(\bar{\boldsymbol{P}}_{\mathrm{int,eq}} - \bar{\boldsymbol{P}}_{\mathrm{int}})$$
$$+ \bar{\Gamma}_{\mathrm{ave}}(\bar{P}_{0\mathrm{int,eq}} - \bar{P}_{0\mathrm{int}})\boldsymbol{z}, \quad (10)$$

where

$$\boldsymbol{P}_{\mathrm{int}} \equiv \int dV_q\boldsymbol{P}, \quad (11)$$

and Γ_{ave} denotes the collision rate at the average energy of neutrinos. Throughout this section, we omit to show these subscripts.

For convenience, we discuss the collisional swap based on $\boldsymbol{S} \equiv \boldsymbol{P} + \bar{\boldsymbol{P}}$ and $\boldsymbol{D} \equiv \boldsymbol{P} - \bar{\boldsymbol{P}}$ instead of $\boldsymbol{P}$ and $\bar{\boldsymbol{P}}$. The QKEs can be rewritten in terms of $\boldsymbol{S}$ and $\boldsymbol{D}$ as

$$\dot{\boldsymbol{S}} \sim \mu\boldsymbol{D} \times \boldsymbol{S} + \frac{\Gamma + \bar{\Gamma}}{2}(\boldsymbol{S}_{\mathrm{eq}} - \boldsymbol{S} + (S_{0,\mathrm{eq}} - S_0)\boldsymbol{z})$$
$$+ \frac{\Gamma - \bar{\Gamma}}{2}(\boldsymbol{D}_{\mathrm{eq}} - \boldsymbol{D} + (D_{0,\mathrm{eq}} - D_0)\boldsymbol{z}), \quad (12)$$

$$\dot{\boldsymbol{D}} \sim \frac{\Gamma - \bar{\Gamma}}{2}(\boldsymbol{S}_{\mathrm{eq}} - \boldsymbol{S} + (S_{0,\mathrm{eq}} - S_0)\boldsymbol{z})$$
$$+ \frac{\Gamma + \bar{\Gamma}}{2}(\boldsymbol{D}_{\mathrm{eq}} - \boldsymbol{D} + (D_{0,\mathrm{eq}} - D_0)\boldsymbol{z}). \quad (13)$$

In the initial condition, $\boldsymbol{S}$ is headed in the positive direction along the z axis (but slightly tilted from the z axis due to perturbations), while $\boldsymbol{D}$ is embedded in the x-y plane (i.e., $D_z = 0$), and its x and y components represent initial perturbations.

Here we consider reasonable approximations in Eqs. (12) and (13) so as to make the problem analytically tractable. We assume that neutrino self-interactions are much stronger than neutrino-matter interactions, which guarantees $t_{\mathrm{CFI}} \ll t_{\mathrm{col}}$. Since the collisional swap occurs in nonlinear phases of CFI, its dynamical timescale is also t_{CFI}. This indicates that, given our initial conditions, $S_0 \sim S_{0,\mathrm{eq}}$, $D_0 \sim D_{0,\mathrm{eq}}$, and $|\boldsymbol{S}| \gg |\boldsymbol{D}|$ are reasonable approximations during the collisional swap. By using these conditions, we can approximate Eqs. (12) and (13) as
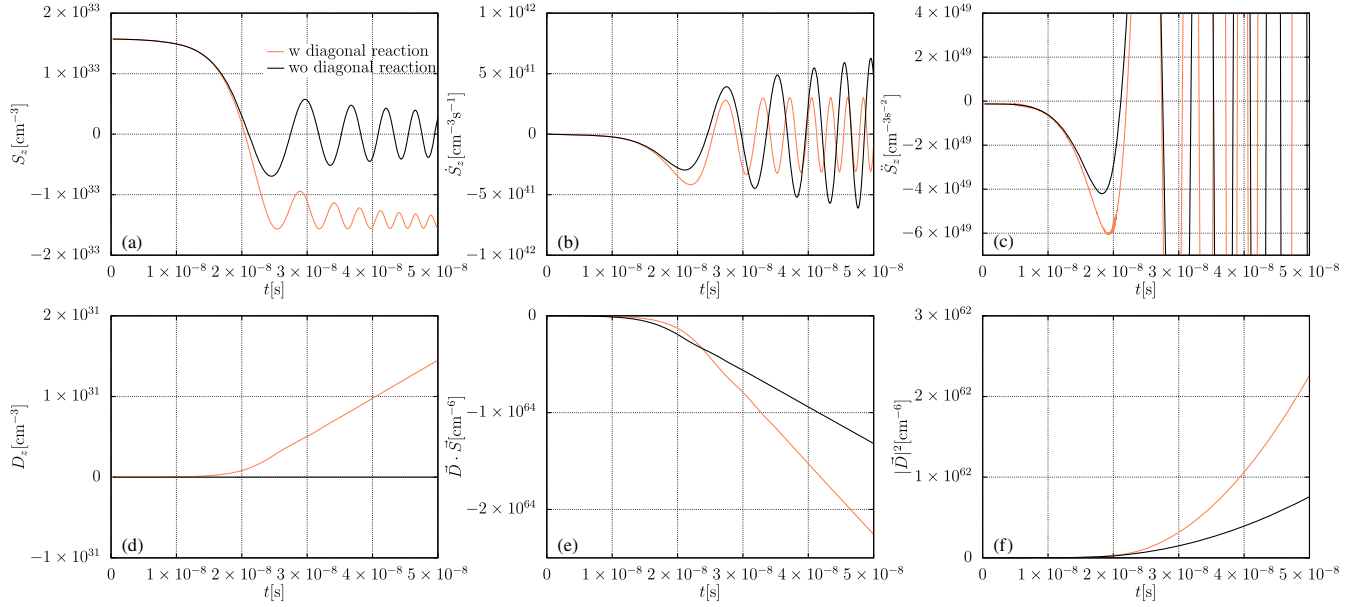
FIG. 2.   Time evolution of (a) S_z, (b) $\dot{S}_z$, (c) $\ddot{S}_z$, (d) D_z, (e) $\boldsymbol{D} \cdot \boldsymbol{S}$, and (f) $|\boldsymbol{D}|^2$. Red and black lines denote cases with and without diagonal components of collision terms, respectively.

$$\dot{\boldsymbol{S}} \approx \mu \boldsymbol{D} \times \boldsymbol{S}, \tag{14}$$

$$\dot{\boldsymbol{D}} \approx \frac{\Gamma - \bar{\Gamma}}{2}(\boldsymbol{S}_{\mathrm{eq}} - \boldsymbol{S}). \tag{15}$$

From Eqs. (14) and (15), we obtain the following relations:

$$|\boldsymbol{S}| \approx |\boldsymbol{S}_{\mathrm{eq}}|, \tag{16}$$

$$\dot{D}_z \approx \frac{\Gamma - \bar{\Gamma}}{2}(|\boldsymbol{S}| - S_z), \tag{17}$$

$$q\partial_t(\boldsymbol{D} \cdot \boldsymbol{S}) \approx \frac{\Gamma - \bar{\Gamma}}{2}(\boldsymbol{S} \cdot \boldsymbol{S}_{\mathrm{eq}} - |\boldsymbol{S}|^2), \tag{18}$$

$$\dot{|\boldsymbol{D}|^2} \approx (\Gamma - \bar{\Gamma})(D_z|\boldsymbol{S}| - \boldsymbol{D} \cdot \boldsymbol{S}), \tag{19}$$

$$\ddot{S}_z \approx \mu^2(\boldsymbol{D} \cdot \boldsymbol{S})D_z - \mu^2|\boldsymbol{D}|^2 S_z, \tag{20}$$

which highlight essential features of collisional swap. It should be stressed that these relations hold in nonlinear phases (but $t \ll t_{\mathrm{col}}$).

Equation (14) guarantees that the norm of $\boldsymbol{S}$ is constant in time; hence it can be given by the initial condition [Eq. (16)]. On the other hand, D_z monotonically increases with time, which can be derived from Eq. (17) with conditions of $\Gamma > \bar{\Gamma}$ and $|\boldsymbol{S}| > S_z$. This also indicates that D_z becomes positive at $t > 0$ [see also Fig. 2(d)]. The trend is also intuitively understandable as follows. Once flavor conversions happen, both ν_e and $\bar{\nu}_e$ are reduced. The restoring force of ν_e to the equilibrium state (i.e., ν_e emission) is stronger than $\bar{\nu}_e$ due to $\Gamma > \bar{\Gamma}$, accounting

for the increase of D_z. Using similar arguments, $\boldsymbol{D} \cdot \boldsymbol{S}$ decreases with time, implying that it becomes negative at $t > 0$ [see also Fig. 2(e)]. We can also derive that $|\boldsymbol{D}|^2$ monotonically increases with time from Eq. (19) and the above relations [see also Fig. 2(f)].

The time evolution of $\boldsymbol{S}$, in particular, for the z component, exhibits the dynamics of collisional swap in Fig. 2(a). Here, we focus on its second derivative [see Eq. (20)]. The first term in the right-hand side of Eq. (20) is negative, because of $\boldsymbol{D} \cdot \boldsymbol{S} < 0$ and $D_z > 0$ at $t > 0$. As a result, S_z separates from the z axis initially, i.e., facilitating flavor conversions. The second term also accelerates the flavor conversion (since it is negative) until $S_z = 0$, implying that $\boldsymbol{S}$ falls to the x-y plane without undergoing decelerations. When $\boldsymbol{S}$ reaches the x-y plane, it still moves toward the negative direction of z axis [see Fig. 2(b) at $t \lesssim 2.5 \times 10^{-8}$ s]. After $S_z < 0$, however, the second term on the right-hand side of Eq. (20) flips the sign, i.e., decelerating flavor conversions. On the other hand, the first term remains negative, implying that S_z is persistently pushed toward $-|\boldsymbol{S}|$ (i.e., flavor swap). The competition between the first and second terms causes S_z oscillation [see also Fig. 2(c)], but the persistent force by the first term makes the system settle into $S_z/|\boldsymbol{S}| \sim -1$, leading to the flavor swap.

As described above, the first term on the right-hand side of Eq. (20) is a key player to achieve the collisional swap. Here, we show that neglecting diagonal components of collision terms results in a qualitatively different outcome. This is attributed to the fact that Eq. (17) in the case is rewritten as

$$\dot{D}_z \sim 0. \tag{21}$$

This indicates that $D_z(=0)$ is constant in time, and consequently, the first term on the right-hand side of Eq. (20) (which is not changed in the case without diagonal components of collision terms) remains to be zero at $t \geq 0$ [see also Fig. 2(d)]. This also implies that $\mathbf{D}$ is always embedded in the x-y plane, making S_z oscillate between positive and negative, since $\mathbf{S}$ rotates around $\mathbf{D}$ [see Eq. (14)].

A few remarks are in order. The first term on the right-hand side of Eq. (20) can be negative only if $D_z \ll S_z$. This is attributed to the fact that $\mathbf{D} \cdot \mathbf{S}$ and D_z have the same sign at $t = 0$, but either of them needs to flip the sign during CFI. This is only possible for cases with $D_z \ll S_z$, i.e., the resonancelike CFI.

Second, the above discussion based on $\mathbf{S}$ and $\mathbf{D}$ can be applied to cases with $\nu_x \neq \bar{\nu}_x$. From the similar argument, the collisional swap can occur, if the condition of resonancelike CFI is satisfied. This is an important indication for CCSN and BNSM study, since ν_x and $\bar{\nu}_x$ spectra are, in general, different from each other due to high-order corrections of weak interactions (e.g., effects of weak magnetism [49]). The deviation would be more prominent if on-shell muons appear in these environments [50,51].

IV. ENERGY DEPENDENCE

In this section, we discuss the energy dependence of collisional swap. Let us first show the time evolution of S_z for some selected neutrino energies in Fig. 3. As shown in this figure, the collisional swap occurs for all energies of neutrinos, and their time evolution is nearly identical. One might think that this result is counterintuitive because the collision rate, which corresponds to a driving force of collisional swap, depends on energy. Below, we explain why there are less energy-dependent features in collisional swap.
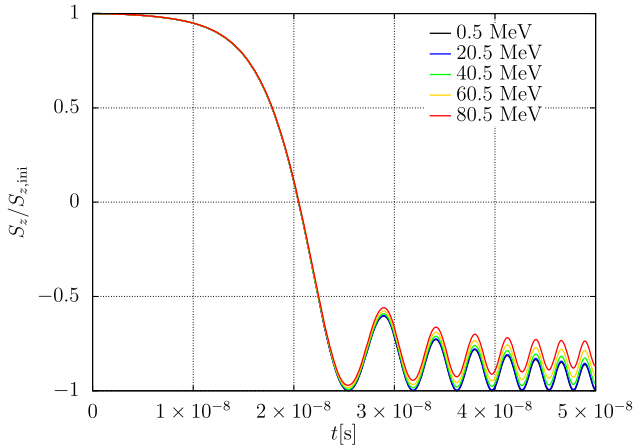

FIG. 3. Time evolution of S_z in each neutrino energy. Colors distinguish neutrino energy. The vertical scale is normalized by the initial value.

One thing we do notice here is that the energy-dependent collision rate affects the dispersion relation for the CFI, but the resultant growth rate of flavor instability is identical among all neutrinos (see, e.g., [28]), which guarantees the energy independence of CFI in the very early phase. However, this explanation is not sufficient for collisional swap, since it occurs beyond the linear phase. We hence consider the energy-dependence directly from the nonlinear QKEs as below.

Similar as in Sec. III, we assume a condition that the neutrino self-interaction is much stronger than neutrino-matter interaction, and we focus on the phase of $t \ll t_{\mathrm{col}}$. These conditions allow us to approximate the time evolution of $\mathbf{S}$ [similar to Eq. (14)] as

$$\dot{\mathbf{s}}(E_\nu) \sim \mu \mathbf{D}_{\mathrm{int}} \times \mathbf{s}(E_\nu), \qquad (22)$$

with $\mathbf{s} \equiv \mathbf{S}/S_{\mathrm{ini},z}$. In this expression, we do not omit the subscript of "int" and we emphasize that $\mathbf{s}$ is defined as an energy-dependent quantity by explicitly showing neutrino energy E_ν. As can be seen in Eq. (22), the time evolution of $\mathbf{s}$ is driven by the energy-integrated quantity $\mathbf{D}_{\mathrm{int}}$. We also note that all neutrino energies have the identical initial condition, $\mathbf{s} = (\xi_x, \xi_y, 1)$, where ξ_x and ξ_y represent the initial small perturbations in x and y components, respectively. This argument guarantees that the time evolution of $\mathbf{s}$ is identical among all energies. We can also obtain the time evolution of s_z as

$$|\mathbf{s}| \approx 1, \qquad (23)$$

$$\ddot{s}_z \approx \mu^2(\mathbf{D}_{\mathrm{int}} \cdot \mathbf{s}) D_{\mathrm{int},z} - \mu^2 |\mathbf{D}_{\mathrm{int}}|^2 s_z, \qquad (24)$$

which are essentially the same as Eqs. (16) and (20). We can apply the same argument as described in Sec. III, and consequently, s_z can reach -1, which exhibits the energy-independent collisional swap. One of the important points along this discussion is that $\mathbf{D}(E_\nu)$ does not directly contribute to the collisional swap, whereas its energy-integrated quantity $\mathbf{D}_{\mathrm{int}}$ is responsible for it. This argument also illustrates that the energy dependence of Γ and $\bar{\Gamma}$ does not directly affect the collisional swap, and their energy-averaged one affects the swap through the time evolution of $\mathbf{D}_{\mathrm{int}}$ [see Eq. (15)].

The energy dependence of flavor evolution appears after the collisional swap is completed. After completing the swap, flavor conversions subside because the flavor state is stable with respect to the CFI. On the other hand, it cannot be an asymptotic state because charged-current reactions make ν_e and $\bar{\nu}_e$ restore the thermal equilibriums at $t \gtrsim t_{\mathrm{col}}$. This trend is clearly displayed in Fig. 4, in which the time evolution of ν_e for some selected neutrino energies are portrayed. At the initial phase, ν_e undergoes a collisional swap regardless of neutrino energies, and then they return to the initial position at $t \gtrsim t_{\mathrm{col}}$. Such a late time evolution
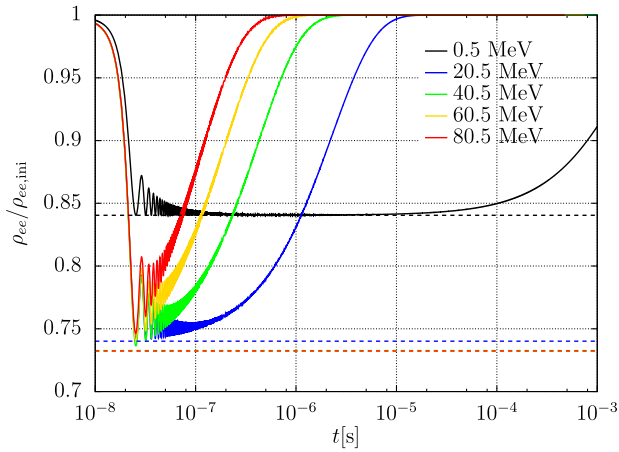
FIG. 4. Long-term evolution of ν_e in each neutrino energy. Colors represent neutrino energy. The vertical scale is normalized by the initial value. To guide our eyes, we also show the initial value of ν_x with dashed lines, and the color code is the same as ν_e.

of neutrinos naturally generates the energy-dependent features, since the restoring speed hinges on the reaction rate.

This argument suggests that an intriguing possibility, spectral swap, may arise in real CCSN and BNSM environments. One thing we do notice here is that the low-energy ν_e and $\bar{\nu}_e$ would not reach their equilibrium states in realistic systems, because the advection timescale is shorter than the collision one. As a result, ν_e and $\bar{\nu}_e$ energy spectra in the low-energy region cannot be restored and they would remain to be depleted, which may form a spectral-swap-like structure.

It should be noted, however, that there remain some uncertainties for this spectral swap phenomenon associated with collisional swap. For instance, the canonical spectral swap involves a discrete change of energy spectrum (see, e.g., [32,33]), but the survival probability of neutrinos should change continuously in the energy spectrum for cases with collisional swap.[2] We also note that there are other elements (e.g., other neutrino-matter interactions) that make the transition smooth. Although this phenomenon is worthy of further investigation, the consistent treatment of

---

[2]We note that the canonical spectral swap would also be smoothed by multiangle effects as demonstrated in [52].

neutrino advection, multiple channels of neutrino-matter interactions, and flavor conversions is necessary to address this issue. We leave the detailed study for a future work.

V. CONCLUSIONS

We present that neutrino-matter interactions can lead to neutrino-flavor swap between two flavors, aided by neutrino self-interactions. Different from the linear phase, diagonal components of collision terms play a key role in the dynamics. The necessary condition for the collisional swap is a resonancelike CFI, which is realized when both ν_e and $\bar{\nu}_e$ number densities are nearly equal to each other (under the assumption of $\nu_x = \bar{\nu}_x$). We also find that the collisional swap occurs regardless of neutrino energies, as long as neutrino self-interactions are much stronger than the collision rate at each energy.

The collisional swap corresponds to the most extreme case in flavor conversions, and it would change the equilibrium state among neutrinos and fluids. We also note that the large flavor conversions in optically thick regions facilitate neutrino cooling [25], which would have substantial impact on CCSN and BNSM dynamics. In fact, resonancelike CFIs have been observed in recent simulations, see, e.g., [27]. The present study also shows that the phenomenon similar to the spectral swap could emerge in the late phase (after the collisional swap is completed), although more work is needed to quantify how much the survival probability is changed in the energy spectrum and how much it can affect the astrophysical consequences. These important issues will be addressed in our forthcoming papers.

---

[1] J. Pantaleone, Neutrino oscillations at high densities, Phys. Lett. B **287**, 128 (1992).

[2] S. Samuel, Neutrino oscillations in dense neutrino gases, Phys. Rev. D **48**, 1462 (1993).

[3] G. Sigl and G. Raffelt, General kinetic description of relativistic mixed neutrinos, Nucl. Phys. **B406**, 423 (1993).

[4] G. Sigl, Neutrino mixing constraints and supernova nucleosynthesis, Phys. Rev. D **51**, 4035 (1995).

[5] B. Dasgupta, A. Mirizzi, and M. Sen, Fast neutrino flavor conversions near the supernova core with realistic flavor-dependent angular distributions, J. Cosmol. Astropart. Phys. 02 (2017) 019.

[6] I. Tamborra, L. Hüdepohl, G. G. Raffelt, and H.-T. Janka, Flavor-dependent neutrino angular distribution in core-collapse supernovae, Astrophys. J. **839,** 132 (2017).

[7] H. Nagakura, T. Morinaga, C. Kato, and S. Yamada, Fast-pairwise collective neutrino oscillations associated with asymmetric neutrino emissions in core-collapse supernovae, Astrophys. J. **886,** 139 (2019).

[8] M. Delfan Azari, S. Yamada, T. Morinaga, W. Iwakami, H. Okawa, H. Nagakura, and K. Sumiyoshi, Linear analysis of fast-pairwise collective neutrino oscillations in core-collapse supernovae based on the results of Boltzmann simulations, Phys. Rev. D **99,** 103011 (2019).

[9] M. Delfan Azari, S. Yamada, T. Morinaga, H. Nagakura, S. Furusawa, A. Harada, H. Okawa, W. Iwakami, and K. Sumiyoshi, Fast collective neutrino oscillations inside the neutrino sphere in core-collapse supernovae, Phys. Rev. D **101,** 023018 (2020).

[10] T. Morinaga, H. Nagakura, C. Kato, and S. Yamada, Fast neutrino-flavor conversion in the preshock region of core-collapse supernovae, Phys. Rev. Res. **2,** 012046 (2020).

[11] S. Abbar, H. Duan, K. Sumiyoshi, T. Takiwaki, and M. C. Volpe, Fast neutrino flavor conversion modes in multidimensional core-collapse supernova models: The role of the asymmetric neutrino distributions, Phys. Rev. D **101,** 043016 (2020).

[12] S. Abbar, Searching for fast neutrino flavor conversion modes in core-collapse supernova simulations, J. Cosmol. Astropart. Phys. 05 (2020) 027.

[13] F. Capozzi, M. Chakraborty, S. Chakraborty, and M. Sen, Mu-tau neutrinos: Influencing fast flavor conversions in supernovae, Phys. Rev. Lett. **125,** 251801 (2020).

[14] H. Nagakura, A. Burrows, L. Johns, and G. M. Fuller, Where, when, and why: Occurrence of fast-pairwise collective neutrino oscillation in three-dimensional core-collapse supernova models, Phys. Rev. D **104,** 083025 (2021).

[15] A. Harada and H. Nagakura, Prospects of fast flavor neutrino conversion in rotating core-collapse supernovae, Astrophys. J. **924,** 109 (2022).

[16] R. Akaho, A. Harada, H. Nagakura, W. Iwakami, H. Okawa, S. Furusawa, H. Matsufuru, K. Sumiyoshi, and S. Yamada, Protoneutron star convection simulated with a new general relativistic Boltzmann neutrino radiation-hydrodynamics code, Astrophys. J. **944,** 60 (2023).

[17] Z. Xiong, M.-R. Wu, G. Martínez-Pinedo, T. Fischer, M. George, C.-Y. Lin, and L. Johns, Evolution of collisional neutrino flavor instabilities in spherically symmetric supernova models, Phys. Rev. D **107,** 083016 (2023).

[18] H. Nagakura, Roles of fast neutrino-flavor conversion on the neutrino-heating mechanism of core-collapse supernova, Phys. Rev. Lett. **130,** 211401 (2023).

[19] M.-R. Wu, I. Tamborra, O. Just, and H.-T. Janka, Imprints of neutrino-pair flavor conversions on nucleosynthesis in ejecta from neutron-star merger remnants, Phys. Rev. D **96,** 123015 (2017).

[20] M.-R. Wu and I. Tamborra, Fast neutrino conversions: Ubiquitous in compact binary merger remnants, Phys. Rev. D **95,** 103007 (2017).

[21] M. George, M.-R. Wu, I. Tamborra, R. Ardevol-Pulpillo, and H.-T. Janka, Fast neutrino flavor conversion, ejecta properties, and nucleosynthesis in newly-formed hypermassive remnants of neutron-star mergers, Phys. Rev. D **102,** 103015 (2020).

[22] X. Li and D. M. Siegel, Neutrino fast flavor conversions in neutron-star postmerger accretion disks, Phys. Rev. Lett. **126,** 251101 (2021).

[23] S. Richers, Evaluating approximate flavor instability metrics in neutron star mergers, Phys. Rev. D **106,** 083005 (2022).

[24] E. Grohs, S. Richers, S. M. Couch, F. Foucart, J. P. Kneller, and G. C. McLaughlin, Neutrino fast flavor instability in three dimensions for a neutron star merger, Phys. Lett. B **846,** 138210 (2023).

[25] H. Nagakura, Global features of fast neutrino-flavor conversion in binary neutron star merger, Phys. Rev. D **108,** 103014 (2023).

[26] J. Liu, R. Akaho, A. Ito, H. Nagakura, M. Zaizen, and S. Yamada, Universality of the neutrino collisional flavor instability in core-collapse supernovae, Phys. Rev. D **108,** 123024 (2023).

[27] Z. Xiong, L. Johns, M.-R. Wu, and H. Duan, Collisional flavor instability in dense neutrino gases, Phys. Rev. D **108,** 083002 (2023).

[28] J. Liu, M. Zaizen, and S. Yamada, A systematic study on the resonance in collisional neutrino flavor instability, Phys. Rev. D **107,** 123011 (2023).

[29] L. Johns, Collisional flavor instabilities of supernova neutrinos, Phys. Rev. Lett. **130,** 191001 (2023).

[30] L. Johns and Z. Xiong, Collisional instabilities of neutrinos and their interplay with fast flavor conversion in compact objects, Phys. Rev. D **106,** 103029 (2022).

[31] Y.-C. Lin and H. Duan, Collision-induced flavor instability in dense neutrino gases with energy-dependent scattering, Phys. Rev. D **107,** 083034 (2023).

[32] H. Duan, G. M. Fuller, J. Carlson, and Y.-Z. Qian, Simulation of coherent nonlinear neutrino flavor transformation in the supernova environment: Correlated neutrino trajectories, Phys. Rev. D **74,** 105014 (2006).

[33] H. Duan, G. M. Fuller, J. Carlson, and Y.-Z. Qian, Neutrino mass hierarchy and stepwise spectral swapping of supernova neutrino flavors, Phys. Rev. Lett. **99,** 241802 (2007).

[34] Z. Xiong, A. Sieverding, M. Sen, and Y.-Z. Qian, Potential impact of fast flavor oscillations on neutrino-driven winds and their nucleosynthesis, Astrophys. J. **900,** 144 (2020).

[35] O. Just, S. Abbar, M.-R. Wu, I. Tamborra, H.-T. Janka, and F. Capozzi, Fast neutrino conversion in hydrodynamic simulations of neutrino-cooled accretion disks, Phys. Rev. D **105,** 083024 (2022).

[36] R. Fernández, S. Richers, N. Mulyk, and S. Fahlman, Fast flavor instability in hypermassive neutron star disk outflows, Phys. Rev. D **106,** 103003 (2022).

[37] J. Ehring, S. Abbar, H.-T. Janka, G. Raffelt, and I. Tamborra, Fast neutrino flavor conversion in core-collapse supernovae: A parametric study in 1D models, Phys. Rev. D **107,** 103034 (2023).

[38] J. Ehring, S. Abbar, H.-T. Janka, G. Raffelt, and I. Tamborra, Fast neutrino flavor conversions can help and hinder neutrino-driven explosions, Phys. Rev. Lett. **131,** 061401 (2023).

[39] S.-i. Fujimoto and H. Nagakura, Explosive nucleosynthesis with fast neutrino-flavour conversion in core-collapse supernovae, Mon. Not. R. Astron. Soc. **519,** 2623 (2023).

[40] S. W. Bruenn, Stellar core collapse—Numerical model and infall epoch, Astrophys. J. Suppl. Ser. **58,** 771 (1985).

[41] S. Furusawa and H. Nagakura, Nuclei in core-collapse supernovae engine, Prog. Part. Nucl. Phys. **129,** 104018 (2023).

[42] S. Furusawa, H. Togashi, H. Nagakura, K. Sumiyoshi, S. Yamada, H. Suzuki, and M. Takano, A new equation of state for core-collapse supernovae based on realistic nuclear forces and including a full nuclear ensemble, J. Phys. G Nucl. Phys. **44,** 094001 (2017).

[43] H. Nagakura, S. Furusawa, H. Togashi, S. Richers, K. Sumiyoshi, and S. Yamada, Comparing treatments of weak reactions with nuclei in simulations of core-collapse supernovae, Astrophys. J. Suppl. Ser. **240,** 38 (2019).

[44] H.-T. Janka, Neutrino emission from supernovae, in *Handbook of Supernovae*, edited by A. W. Alsabti and P. Murdin (Springer International Publishing, Cham, 2017), p. 1575.

[45] C. Kato, H. Nagakura, Y. Hori, and S. Yamada, Neutrino transport with Monte Carlo method. I. Toward fully consistent implementation of nucleon recoils in core-collapse supernova simulations, Astrophys. J. **897,** 43 (2020).

[46] H. Nagakura, A. Burrows, D. Radice, and D. Vartanyan, A systematic study of proto-neutron star convection in three-dimensional core-collapse supernova simulations, Mon. Not. R. Astron. Soc. **492,** 5764 (2020).

[47] R. Akaho, J. Liu, H. Nagakura, M. Zaizen, and S. Yamada, Collisional and fast neutrino flavor instabilities in two-dimensional core-collapse supernova simulation with Boltzmann neutrino transport, Phys. Rev. D **109,** 023012 (2024).

[48] C. Kato, H. Nagakura, and T. Morinaga, Neutrino transport with the Monte Carlo method. II. Quantum kinetic equations, Astrophys. J. Suppl. Ser. **257,** 55 (2021).

[49] C. J. Horowitz, Weak magnetism for antineutrinos in supernovae, Phys. Rev. D **65,** 043001 (2002).

[50] R. Bollig, H. T. Janka, A. Lohs, G. Martínez- Pinedo, C. J. Horowitz, and T. Melson, Muon creation in supernova matter facilitates neutrino-driven explosions, Phys. Rev. Lett. **119,** 242702 (2017).

[51] T. Fischer, G. Guo, G. Martínez-Pinedo, M. Liebendörfer, and A. Mezzacappa, Muonization of supernova matter, Phys. Rev. D **102,** 123001 (2020).

[52] M.-R. Wu, Y.-Z. Qian, G. Martínez-Pinedo, T. Fischer, and L. Huther, Effects of neutrino oscillations on nucleosynthesis and neutrino signals for an $18M_{\odot}$ supernova model, Phys. Rev. D **91,** 065016 (2015).